International Journal of Thermal Sciences 137 (2019) 299–312

Contents lists available at ScienceDirect

International Journal of Thermal Sciences

journal homepage: www.elsevier.com/locate/ijts

Effects of contact-nature on transient thermal contact conductance

Surya Kumar[a,b], Andallib Tariq[b,*]

[a] Department of Mechanical Engineering, Katihar Engineering College, Katihar, Bihar, 854105, India
[b] AVTAR (Aerodynamics Visualization and Thermal Analysis Research) Lab, Department of Mechanical and Industrial Engineering, Indian Institute of Technology Roorkee, Roorkee, Uttarakhand, 247667, India

ARTICLE INFO

Keywords:
Interfacial heat transfer
Thermal contact conductance (TCC)
Transient TCC
Steady-state TCC
Inverse heat conduction
Conforming contacts
Non-conforming contacts

ABSTRACT

The behaviour of transient interfacial heat transfer across metallic contacts has significant importance in different heat transfer processes of practical importance, viz. casting, forging, smelting, soldering, glass forming etc. Present investigation systematically explores and develops an understanding of the effect of different nature of contacts on transient interfacial heat transfer/thermal contact conductance (TCC). In the present experimental investigation, six different contact configurations which represent conforming as well as non-conforming contacts of steel-steel have been selected towards estimating TCC under three consistent loading conditions. Sequential function estimation (SFE) algorithm utilizing single sensor data has been employed for solving related heat conduction problem (IHCP) using analytical solution for a semi-infinite body. Subsequently transient TCC is determined by the estimated transient average heat flux and instantaneous temperature jump. Results of transient TCC of different contact configurations show a definite effect of nature of contacts on transient TCC. This study suitably explains why different engineering applications show different behaviour of transient TCC under similar thermo-physical conditions. However, transient methodology which aims to determine the time varying estimate of contact heat transfer related with the specific application areas had seldom been used for estimating the steady state TCC. Further, in the present work, quasi-static thermal equilibrium obtained in transient test run, form the basis to successfully extract the steady-state TCC obtained by interfacial temperature drop, calculated without extrapolating the temperature profiles of each contacting body.

1. Introduction

Accurate knowledge of thermal contact conductance (TCC) is becoming increasingly important in major engineering applications ranging from critical areas like nuclear reactor cooling and spacecraft thermal control to the fields of electronics packaging, gas turbine, internal combustion engine cooling, heat exchangers, sample-tool interface, forging and metal forming processes. Due to its immense technological importance, it had been an area of research for several decades. However, correct evaluation of TCC for any contacting surfaces is complex and cannot be measured or calculated directly due to the difficulty in estimating the real contact area between the mating surfaces. A detailed examination of all engineering surfaces shows that they are not perfectly smooth. These surfaces contain a large number of microscopic peak and valleys. If two surfaces are in contact under nominal loading condition, actual contact is made only at a few discrete points separated by relatively large gaps. Consequently, a very limited contact of solid spots results in constriction of heat flow at the interface, known as thermal contact resistance. The reciprocal of thermal contact resistance is called TCC and it is normally defined as:

$$h = \frac{\dot{q}}{\Delta T} \tag{1}$$

where, $\dot{q}$ is the average heat flux passing through the interface, and is the temperature drop occurring at the interface.

Many researchers have carried out significant works on the estimation of thermal contact conductance by using theoretical as well as experimental methods. Some of the pioneer works like CMY model [1] and Mikic model [2] paved the way for analytical works. However, predicting TCC, based upon theoretical models is a tough task due to complexities involved in handling real surface geometries, and associated elastic, plastic and elastoplastic deformations of contacting asperities. Therefore, experimental procedures become a reliable means in predicting TCC for different engineering applications. In regard to the experimental methods, steady or transient approaches are used for evaluating TCC. In the steady state approach, axial steady state temperature distribution of contacting bodies is recorded by means of sensors inserted inside the bodies. The axial temperature distribution is

* Corresponding author.
E-mail address: tariqfme@iitr.ac.in (A. Tariq).

https://doi.org/10.1016/j.ijthermalsci.2018.11.029
Received 24 December 2017; Received in revised form 22 October 2018; Accepted 23 November 2018

used to fit a straight line in each body between temperature and location of sensors. The straight line fit from both the bodies is extrapolated linearly till the interface to get interfacial temperature drop (ΔT) [3]. The steady state TCC is then calculated using estimated $\dot{q}$ and in Equation (1). In the transient heat transfer, temperatures of the contacting bodies vary with time, and an understanding of the complete time history of the temperature variation is required.

Published works on steady and transient TCC can be classified into two groups. In the first group of studies, researchers have chosen their experimental approach based on the nature of thermal loading experienced by the contacting solids i.e., steady or transient. Steady state experiments are used for the estimation of TCC for fixed contacting solids experiencing steady state heat transfer which is important in application areas related with nuclear reactors, internal combustion engines, electronic packaging, heat exchangers, bolted joints, cryogenic applications [4,5]. Whereas, transient experiments are performed to understand the transient behaviour of interfacial heat fluxes, TCR/TCC, and temperature distributions in the fields of internal combustion engine [6], solidification and casting [7], electroslag remelting [8], quenching [9], glass forming process [10], metallic contacts with different thicknesses of air gap [11]. It was observed in the above works that the transient interfacial heat flux rises immediately at the onset of heat transfer process, and starts decreasing after attainment of the peak. The sharp initial rise in the heat flux were linked with the high heat addition due to the good contact at the onset of various manufacturing processes [7–10], and the peak in the heat flux had been associated with the beginning of respective phase change processes (e.g. nucleate boiling, solidification, etc.). A clear peak is observed in each case of transient interfacial heat flux, whereas, in case of transient TCC, different natures of curves in terms of either peak or flatter profile are observed. In this context, experimental investigation of transient heat transfer between specimens with narrow macroscopic gap [11] showed a sharp rise is TCC curve till attainment of a peak, which decreases gradually with time. Similar phenomenon of obtaining a peak in transient TCC have been observed in different metal forming processes [12]. In most of these studies, the peak value was taken as the representative point to represent TCC. In contrast to these observations, Malinowski et al. [13] estimated the interfacial heat transfer coefficient between workpiece and die interface and observed a fast rate of continuous increase in the transient curves of TCC at higher loading condition. Whereas, a much slower rise of TCC leading to almost a stabilized flatter profile without any peak was observed at lower contact pressures. In these investigations, a conflicting perspective does occur in selecting the representative value of TCC from its variation curve. Whenever, a peak is attained in these results, the value of the peak was generally taken as the representative value of the TCC. However, no clear representation of TCC emerges out of the curves carrying flatter profiles. Therefore, the occurrence of different nature of transient TCC variation needs a proper assessment to understand transient behaviour of TCC found in different engineering applications.

In the second group of studies, researchers [6,14] have focussed on the merits and demerits of steady and transient approaches based on experimental duration. Experimental determination of steady state TCC is reported as the most reliable method in TCC estimation [5,15], but its drawback has also been highlighted, which is the long hour of waiting time in settling of heat transfer through the contacting specimens. Whereas, transient experiments are considered a very fast approach for the TCC estimation [6,16]. Transient experimentation is shown as the superior approach over steady state to estimate TCC. However, the value of TCC obtained from transient analysis can be used or not to represent steady state TCC, remained unanswered in the published works. Some attempts [6,13,17] have been made in the past, in acquiring the equivalent of steady state TCC value from the transient experimental analysis. Fieberg and Kneer [6] estimated the TCC with the help of very short duration transient experiments (1.4 s), while using high speed infrared thermography (IRT); but the result shows a remarkable deviation from the analytical correlations. In another work [17], after the rapid rise, a slow and continuous increasing trend in TCC had been observed till a longer test time (upto 40 s). However, concerns were raised that, if the test time would had been much long enough, can the thermal contact conductance reach a steady state value? In these works, stabilized value of transient TCC is considered as the steady state TCC, without any comparison with the TCC obtained from the steady state experimentation. Additionally, there is no published data which show a steady state apparatus and a transient apparatus simultaneously being used to produce the same result. Apart from the disagreement between TCC obtained from transient experimentation and TCC obtained from correlations, conflict also exists in these works in deciding the stabilized zone/value of TCC from transient TCC variations. These underlying issues calls for a comparative study between the transient and steady state TCC measurements performed on same specimen/setup in order to predict steady state TCC using transient measurements.

Most of the steady and transient experiments are executed for flat-flat or surface contacts, whereas very limited amount of investigations were performed on curvilinear contacts for steady state as well as transient studies. Therefore, the role of curvatures at the contact has not been adequately understood even though these contacts have diverse applications in the field of space structures, air conditioning systems, pipelines, plug and ring assemblies, shrink-fit cylinders, finned tube heat exchangers, nuclear reactor fuel elements and bearings [18,19]. Madhusudana [20] presented an analysis for the prediction of the thermal conductance of cylindrical joints for radial heat flow. The TCC was shown to be dependent on the geometrical, thermos-physical and surface properties of the cylinders as well as heat flux and maximum operating temperatures. Kumar et al. [19] developed a mathematical model to predict TCC between curvilinear surfaces and conducted experiments in vacuum for the measurement of TCC between stainless steel and aluminium cylindrical contacts over a range of nominal pressure. It was found that the value of TCC is of lower magnitude in cylindrical contacts as compared to flat contacts. Mcgee et al. [21] presented a line contact model for the thermal resistance of a cylinder-flat contact, and compared the results with the experimental measurements. It was observed that the validity of line-contact model was dependent on minimal contact loading condition, and large errors were reported below a certain value of load parameter. Complexity of this particular field calls for reliable experimental investigations to predict the TCC for different curvilinear contacts.

The present work is a systematic effort towards estimating transient TCC between different types of metallic contacts under consistent loading conditions. Both the experiments, i.e. steady and transients have been performed on the same experimental setup to have a better comparison between their results. Results obtained from the exhaustive sets of transient experiments and their corresponding steady state experiments performed on the same contacts of different geometric configurations have been discussed in detail. Sequential function inverse algorithm based on 1-D semi-infinite conduction solution using single sensor measurements has been implemented for the estimation of transient TCC. Transient experiments have been performed over six different types of contact configurations to explore the effect of contacts on the nature of interfacial heat transfer under different loading conditions. Geometrical configurations have been selected in such a way that all types of contact can be studied, i.e. conforming (surface) and non-conforming (line). Schematic of typical conforming and non-conforming configuration with their contacting and non-contacting ends is shown in Fig. 1. The duration of the transient heat transfer experiments were selected judiciously as per the validity criteria of semi-infinite solid assumption, i.e. the total duration of the transient run should be lesser than the penetration time of the substrate $t \leq 0.1\, x^2/\alpha$ [22]. A simple calculation using standard thermo-physical properties of specimen reveals that the maximum permissible penetration time in the present case is ≤ 40 sec.

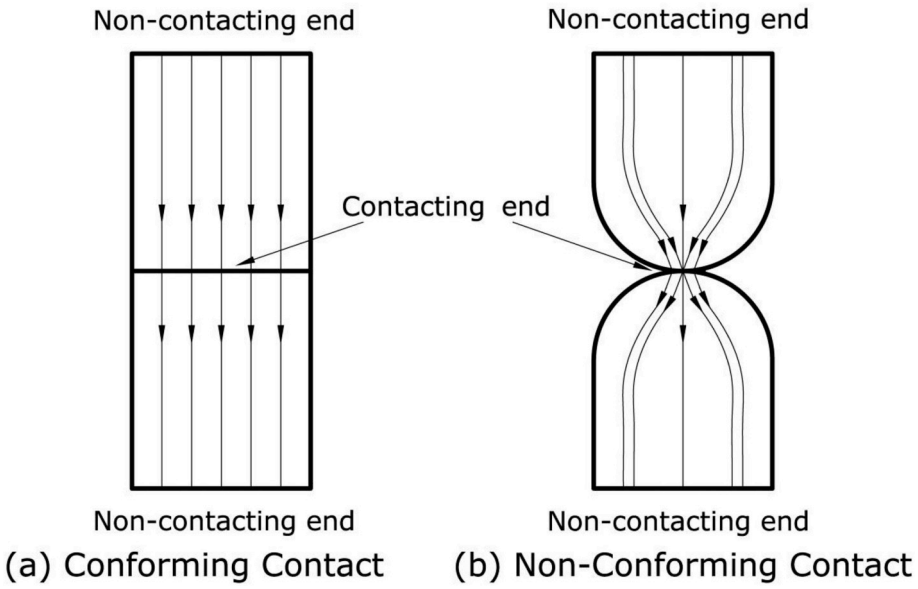

Fig. 1. Contacting and non-contacting ends of (a) conforming contact and (b) non-conforming contact.

Summarizing, the scopes of the present work, three major objectives are simultaneously dealt in this paper. The main focus is to estimate the transient variation of TCC at the interface of different contact configurations. The second objective is to compare the results of transient variation with the steady state TCC for the same metallic contacts. The last one is to present a data base for the transient and steady state TCC for different geometrical configurations consisting surface as well as line contacts. The comparison of the transient results against the steady state measurements on the same and well standardised setup can be treated as the unique strength of the investigation, which is seldom addressed in the literature. The comparison of transient with steady state results of each geometrical configuration obtained from same experimental setup ensures the reproducibility of the outcome; and henceforth can be treated as the benchmark dataset for any of the upcoming theoretical models in the pertinent field.

2. Inverse heat conduction problem

Due to the difference of physical process between steady state and transient heat transfer, linear extrapolation of temperature profile used in steady state TCC estimation can't be used to estimate transient TCC. In the current work, linear least squares error method has been used for solving inverse heat conduction problem (IHCP) in estimating transient TCC. The inverse heat conduction problem implies that the effect (temperature at interior locations in both the bodies) is utilized to estimate the cause (interfacial boundary condition, i.e. TCC). Inverse problem can also be described in terms of an optimization problem where the objective function is represented by the squared difference between measured and estimated unknown variables.

In an IHCP, boundary conditions, initial conditions, or thermophysical properties of material are not fully specified, and they are determined from temperature measurement of the internal location of the body. The challenge is that the effect of the transient temperature response of an internal point in a heat conducting body is lagged and damped compared to the changes in the boundary condition of the body [23], i.e. the varying magnitude of the interior temperature profile lags behind the changes in boundary conditions and is generally of lesser magnitude. Therefore, IHCP is categorized as an ill-posed problem, and it is very sensitive to measurement errors. Its solution becomes unstable if small perturbations in the input data result in large oscillations in the output [24]. As all experimentally-based IHCPs will have inherent perturbations in the data, owing to measurement errors, therefore a regularization method is used for the stability of its solution.

Beck and Woodbury [25] presented regularization methods used in the solution of IHCPs. Some of the prominent methods are Tikhonov regularization, iterative regularization and function specification. Function specification method is simpler in concept and implementation than the other two regularization methods mentioned above. It is also computationally very efficient, as in this method, functions can be found one component at a time, whereas in other two regularization methods unknown function is found in a whole-domain fashion i.e., all the components are estimated simultaneously [26].

The conventional way to add regularization to inverse problems is by minimizing the error between the computed data and the measured data with respect to the unknown function [27]. The earliest IHCP method, developed by Stoltz [28], involved the computation of heat flux component at a given time by setting the calculated temperature equal to the measured temperature at that time. This “exact matching” method is highly susceptible to noise in the input data, particularly as the data time step becomes small [23]. In an improvement to Stoltz method, Beck et al. [26] has introduced ‘several future time steps’ to regularize the IHCP algorithm. Beck et al. [26] had introduced the concept of using lesser number of data points from the total data points for the estimation of function by temporarily assuming that function (interfacial heat flux) fixed over the unused data sets. The uses of lesser number of data points give more data without introducing more unknowns. The number of unused data/measurement is termed as the future time steps/temperatures. In this paper, sequential function estimation (SFE) algorithm developed by Beck et al. [26] has been used to solve IHCP. Here a functional form of the interfacial heat flux variation with time is assumed, and the unknown parameters in the assumed functional form are found sequentially at each time step. The concept of several future time steps has been used for the regularization of SFE algorithm.

The intrusive way of internal temperature measurements, and the mounting of multiple sensors in the heat conducting bodies disturbs/modify the very thermophysical phenomena responsible for the ensuing heat flux transport [29]. Because of this drawback, inverse estimation of interfacial heat flux using single sensor measurements has been recommended [26]. It utilizes the measurement of single sensor in solving the unknown, where the use of several future temperatures greatly improves the stability of the algorithm and substantially reduces the sensitivity to measurement errors.

2.1. IHCP formulation

The determination of unknown boundary condition, $h(t)$ is not possible at the inaccessible interface through the solution of direct heat conduction problem. Therefore, the estimation of TCC is based on the solution of IHCP utilizing the experimental transient temperature data. A sequential function estimation method has been used to solve IHCP problem. It estimates the interfacial heat flux, $\dot{q}(t)$. The estimation of $\dot{q}(t)$ is based on the analytical solution for a semi-infinite body. Although hot body and cold body are finite in dimensions, but if the contact span is considered to be extremely short as against the penetration time of the substrate, then the bodies can be treated as being semi-infinite, and the classical solution of semi-infinite conduction problem with prescribed initial surface temperature, and boundary conditions can be used to evaluate the unknown interfacial heat flux, $\dot{q}(t)$ at the interface. The transient 1-D heat conduction equation along with boundary and initial condition for a semi-infinite body, while considering the constant properties can be written as:

$$\frac{\partial T}{\partial t} = \alpha \frac{\partial^2 T}{\partial x^2} \qquad \frac{\partial T}{\partial x} = 0 \text{ , } when\ x \rightarrow \infty$$
$$\dot{q} = -k \frac{\partial T}{\partial x}\ at\ x = 0 \qquad T(x, t = 0) = T_i \tag{2}$$

Material properties and data used in solving inverse problem are summarized in Table 1. Further to evaluate the TCC from Eq. (1), the heat flux across the interfacial boundary has to be calculated. Presently, the sequential function estimation algorithm proposed by Beck et al. [26] has been used for the estimation of $\dot{q}(t)$, which is shown below:

$$\dot{q}(t) = \frac{\sum_{i=1}^{r} (Y_{M+i-1} - \hat{T}_{M+i-1}\Phi_i)}{\sum_{i=1}^{r} \Phi_i^2} \tag{3}$$

Eq. (3) optimizes the least square difference between the measured and calculated temperatures at each time step, based on the sensitivity coefficient. With the step response to a unit heat flux jump for a semi-infinite body, the sensitivity coefficient can be represented by Eq. (4) [30]:

$$\Phi(x,t) = \frac{1}{k}\sqrt{4\alpha t}\left(\frac{1}{\sqrt{\pi}}\exp\left(-\frac{1}{4Fo}\right) - \frac{1}{\sqrt{4Fo}}\operatorname{erfc}\left(\frac{1}{\sqrt{4Fo}}\right)\right) \tag{4}$$

Temperature extracted from single sensor location has been used in the estimation of $\dot{q}(t)$. Subsequently, $h(t)$ for conforming as well as non-conforming contacts has been evaluated from Eq. (1), using the estimated value of $\dot{q}(t)$. The SFE algorithm used in the present work has been extensively tested with the numerically generated data in the authors' earlier work [31].

3. Apparatus and instrumentation

Experiments have been performed in an updated version of uniquely designed set-up [5,32,33] which was fabricated to carry out axial heat flow steady state experiments. Fig. 2 presents the schematic of complete experimental set-up indicating all the attachments. The details of apparatus and instrumentations have been described in an earlier publication and can be referred further [5,32]; however for the sake of completeness, the salient details of the setup used to perform transient and steady state measurements have been briefed in the following paragraphs.

Table 1
Data used in solving the inverse problem.

	Hot Body	Cold Body
Thermal conductivity W/m − K,	16.0	16.0
Thermal diffusivity m^2/s,	4.09 x 10^{-6}	4.09 x 10^{-6}
Initial temperature °C,	37.0 ± 0.25	25.5 ± 0.25
Sensor position m,	0.002	0.002
Future time steps	10	10

The modified setup has a provision to perform transient heat transfer experiments. It consists of a mechanism to separately hold upper and lower specimens. For heating purpose, a cylindrical steel block in which five 150 W high performance cartridge heaters are inserted vertically has been utilized in conjunction with a precise and stable PID controller. The cooling of the lower specimen has been attained by putting it into the thermal contact of a specially designed cooling block made up of copper. Chilled fluid consisting of a mixture of ethylene glycol and water (volume ratio of 40–60) coming out of a specially designed highly precise and stable PID controlled chiller has been re-circulated through this cooling block. An insulation block (Isomag® 175, Spokane Valley, WA, USA) made of magnesium silicate has been placed at the top of heating block and at the bottom of cooling block, to ensure one dimensional heat flow as well as to avoid heat losses. The insulation blocks maintain its high compressive strength and low thermal conductivity up to 1000 °C. In the test column, all the interfaces except the test interface are pasted with a highly conductive silicone paste to reduce the contact resistance of the interfaces and to maximize the heat flow. To perform experiments under different contact pressure, a hydraulic jack arrangement has been fitted beneath the cooling block in combination with the pre-calibrated digital load cell. To maintain the required pressure of the hydraulic circuit, a diaphragm type accumulator along with a check valve has been installed as work holding devices. These two devices have not only minimized any fluctuations in the loading circuit but also ensured constant loading at the interface of two contacting solids during experimental run.

3.1. Test specimens

Stainless steel metal has been selected for all test specimens. Different sets of upper and lower specimen for six different configurations are prepared by using CNC wire cut EDM machine. Highly precise machining has not only produced flat surfaces but also generated precise contour as required for curvilinear geometries. Picture of actual test specimens used in the present work is shown in Fig. 3. The quality of machining can be clearly seen in the prepared specimens where each combination of specimens presents distinct nature of contacts, which is essentially needed for the present investigation.

Temperatures at different axial locations have been measured using fast response K-type ungrounded micro thermocouples (Omegaclad®) of wire diameter, 0.1 mm with sheath diameter of 0.5 mm. Thermocouples have been mounted at the axial locations inside the specimens. The thermocouples have been carefully inserted deep up to the centerline (11.25 mm deep) inside the EDM drilled holes, and to fix the thermocouples, a highly conducting paste has been filled in the holes. The temperature logging has been obtained by a National Instrument NI cDAQ-9178 data acquisition chassis with a NI-9213 module for thermocouple interfacing. The same experimental facility has been used for transient as well as steady state experiments. Thermal conductivity system (TPS 2500S) based on transient plane heat source (TPS) hot disk method has been used for the measurement of thermal properties of specimens.

3.2. Geometrical parameters of contact configurations

Line diagrams representing dimensions and thermocouple positioning of six different contact configurations used in transient and steady state experimentations are shown in Fig. 4. Configuration I and II represent conforming contact and configurations III to VI represent non-contacting configurations. Configurations II to VI have been selected by taking fixed radius geometry of hot/upper body ($R_o^H = -11.5$ mm) and varying the radius of cold/lower body (i.e.− 11.5, −20.0, ∞, +20.0 and + 11.5 mm). In Fig. 5, five configurations (II-VI) are superimposed to illustrate the nature of contacts. Keeping the dimensions of hot body fixed, contour radius of contacting side of cold body has been varied from configuration II till

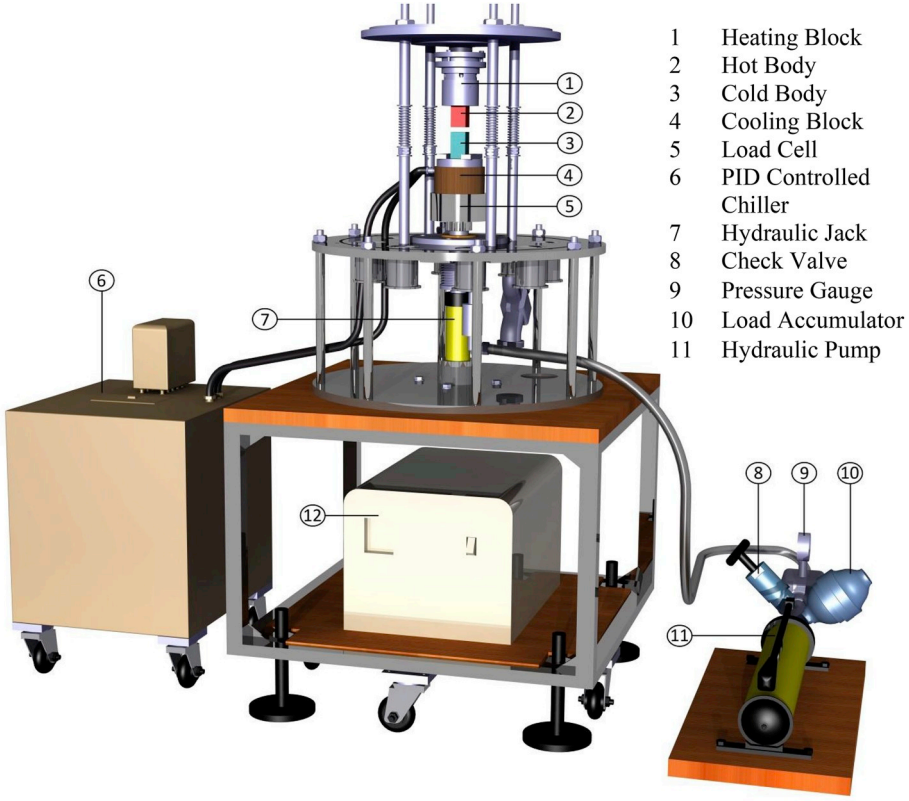

Fig. 2. Schematic representation of actual experimental setup.

configuration VI in the order of reducing contact width. Contact width has been calculated using classical Hertz contact stress [34]. The calculated contact width of each non-conforming contact is given in Table 1. The nature of contacts illustrated in Figs. 4 and 5 forms the basis to study the effect of different nature of contacts on transient TCC.

3.3. Experimental procedure

All the experiments have been executed under ambient condition. Experiments have been performed to record the actual temperature measurements during the transient and steady state run.

3.3.1. Transient

One dimensional transient temperature data at single location in both the specimens has been recorded with time and provided as measured data to the inverse algorithm to estimate transient interfacial heat flux. Initially, upper body is heated and lower body is cooled separately. After attaining the specified initial temperatures, heater and chiller have been switched off and then cold body is brought into contact with the fixed hot body through the stroke of hydraulic jack. After the contact, both the bodies are pressed together to a specified nominal pressure, which ensembles the actual transient runs involved during many of the manufacturing processes in the best possible manner. Transient experiments have been conducted with initial temperature conditions, i.e. 37.0 ± 0.5 and $25.5 \pm 0.5\ ^{\circ}C$ of the hot and cold specimens, respectively for all six configurations. The temperature changes in the contacting bodies have been recorded using single thermocouple mounted inside each of the contacting specimens.

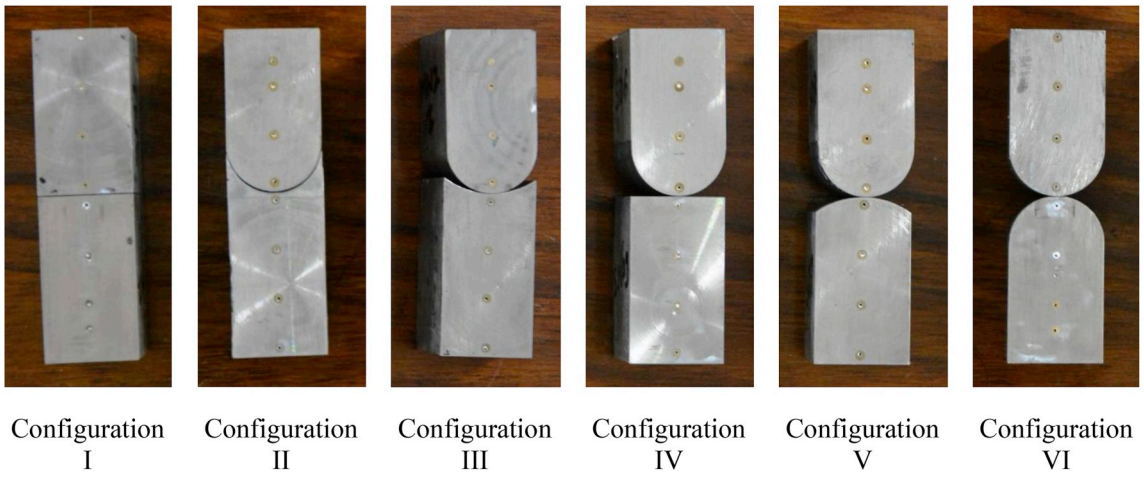

Fig. 3. Photograph of actual test specimens.

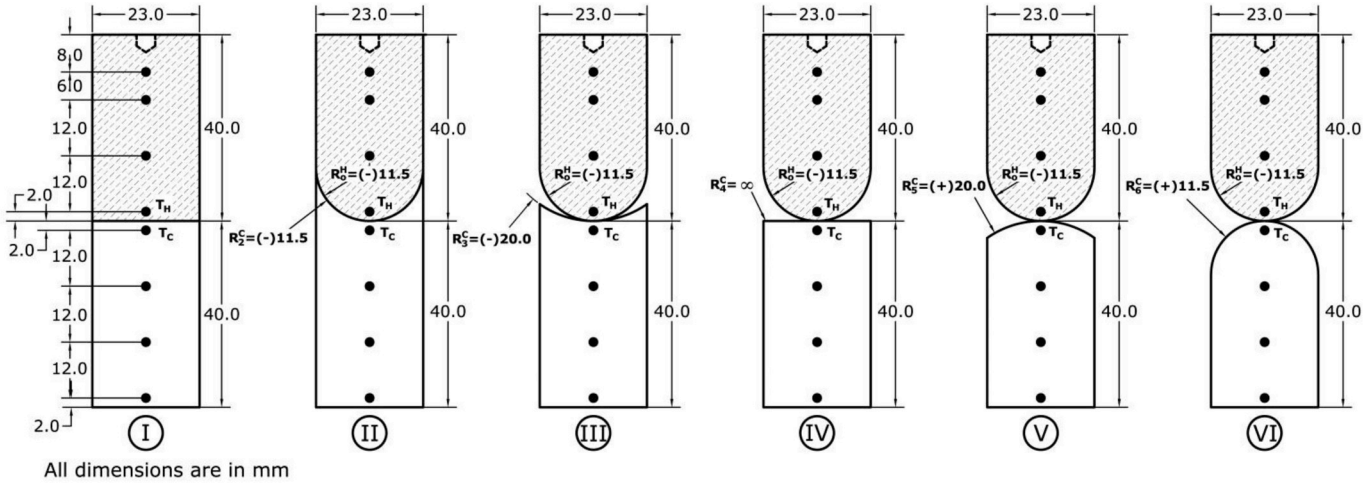

Fig. 4. Contacts of six different geometrical configurations.

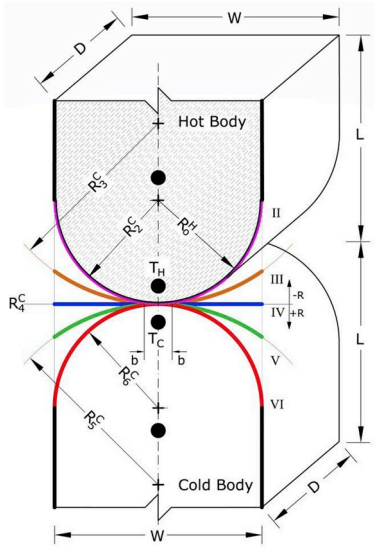

D = 22.5 mm
W = 23.0 mm
L = 40.0 mm
R_o^H = 11.5 mm
R_2^C = 11.5 mm
R_3^C = 20.0 mm
R_4^C = ∞
R_5^C = 20.0 mm
R_6^C = 11.5 mm

Half Width of Contact (Configurations III-VI):

$$b = \sqrt{\frac{2F}{\pi D}\frac{(1/E_{eff})}{\left(1/2R_H^U\right)+\left(1/2R_C^L\right)}}$$

where,

$$E_{eff} = \left[\frac{(1-\nu_U^2)}{E_U} + \frac{(1-\nu_L^2)}{E_L}\right]^{-1}$$

Fig. 5. Variations in the radius of lower body shown by different colours and dimensional detail of geometrical configurations II-VI.

Thermocouples, T_H and T_C is mounted 2.0 mm away from the interface in hot and cold specimens respectively. Transient temperature histories from both the thermocouples (T_H and T_C) have been used to evaluate $\Delta T(t)$ and $\dot{q}(t)$. The transient temperature drop ($\Delta T(t)$) has been calculated by the difference of temperature histories of thermocouples T_H and T_C. The unknown $h(t)$ has been determined by using Eq. (1). The temperature variation of the nearest thermocouples at the non-contacting side has also been recorded simultaneously, which is used to check the time taken for change in temperature by 1.0% at the farthest point from the interface (contacting side). As a thumb rule, time duration until 1.0% of temperature change at the farthest point from the interface is considered as penetration time for the semi-infinite solid.

3.3.2. Steady state

Once transient experiment has been completed, heater and chiller have been restarted and kept under running condition without disturbing the contact of specimens and loading condition, until it attains the steady state condition. The steady state is considered to be achieved; only when the temperature difference at each location is not more than 0.1 °C in 20 min. The value of steady state heat fluxes, $\dot{q}_1$ and $\dot{q}_2$ are measured from upper and lower specimen respectively, while using the classical Fourier's heat conduction law. The average of upper and lower heat fluxes of each specimen is taken as the measure of interfacial heat flux $\dot{q}$. In the conventional and typical way of steady state TCC estimation, linear temperature profile is extrapolated from the last sensor location (in the present case, either from T_H or T_C) to the interface in each contacting body. The steady state temperature drop (ΔT) is then calculated from the difference of extrapolated temperature obtained at the interface from both the bodies. In this work, steady state TCC estimated on the basis of extrapolated measurement, is designated as $h_{\Delta T\_exptrp.}$.

In the transient analysis, no extrapolation of temperature profile has been performed and $\Delta T(t)$ has been calculated exactly at the last sensor location, i.e. T_H or T_C. Therefore, in view of a valid comparison with the transient TCC, the steady state TCC has also been estimated on the basis of temperature drop (ΔT) calculated by the steady state temperature difference between T_H or T_C i.e. direct calculation of temperature drop without performing any extrapolation. In this work, steady state TCC estimated on the basis of direct measurement of , is designated as. $h_{\Delta T\_no\ exptrp.}$

4. Results and discussion

Results obtained from the experiments conducted on six different configurations of stainless steel – stainless steel contact to study the effect of contact configuration on the nature of transient interfacial heat transfer have been discussed in details. This discussion has been further extended at three different loading conditions. It is important to highlight that, due to the complexities of different nature of contact configurations; it is extremely difficult to maintain exactly same nominal loading in all the six configurations. Therefore, the reading of hydraulic gauge pressure is fixed for each of the contact configuration under experimental run. This fixed value is maintained throughout the test run for each contact configurations. Three fixed sets (i.e., 100, 1000 and 2000 psi) of hydraulic pump gauge reading have been selected in the present study. Therefore, results have been discussed for the experiments performed under three fixed sets of loading conditions (i.e., 100, 1000 and 2000 psi) for all six configurations. In the end, transient TCC has been compared with their respective steady state TCC, $h_{\Delta T\_exptrp.}$ as well as $h_{\Delta T\_no\ exptrp.}$ for all the six configurations.

4.1. Transient temperature

Before and after the contact of hot and cold body, the temperature variation with time has been recorded by two thermocouples; one is mounted near the contacting side (interface) and other one is near the non-contacting side in each body. A typical temperature variation at a

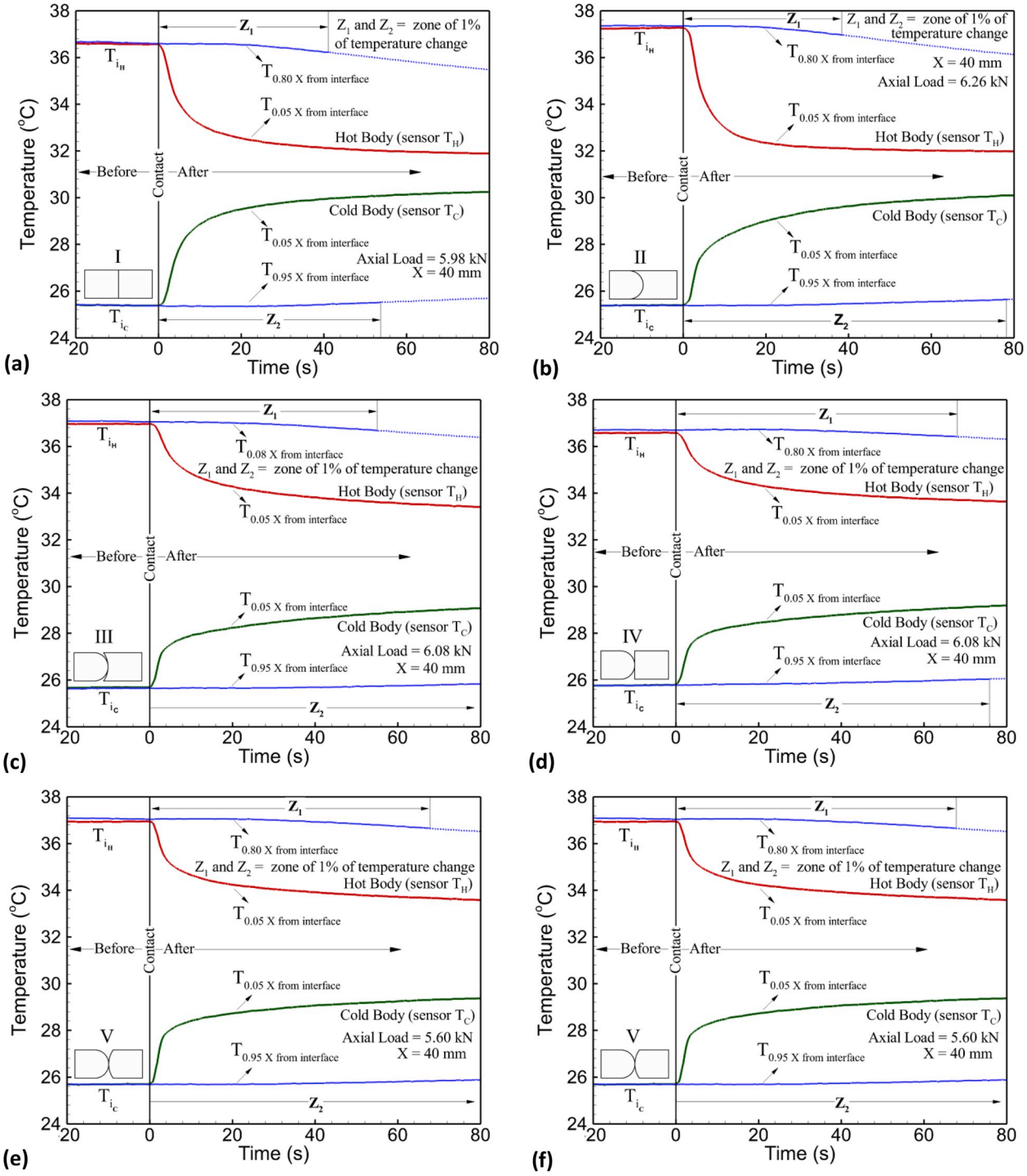

Fig. 6. A typical temperature variation with time in the contacting bodies of stainless steel of (a) configuration I, (b) configuration II, (c) configuration III, (d) configuration IV, (e) configurationV, and (f) configuration VI, under 2000 psi gauge pressure.

loading condition of 2000 psi has been shown for six configurations in Fig. 6. The temperature histories show the ability of ultra-sensitive micro-thermocouples sensors to record high quality temperature measurements. It has been observed that heat flow get initiated from hot to cold bodies at the onset of contact, and a sharp temperature variation in the reading of interfacial thermocouples (T_H and T_C) happens immediately after. After the contact, a sharp temperature gradient can be seen in the configurations I and II whereas gradient gets reduced in other four configurations under similar loading and thermal conditions. The limited contact at the interface in non-conforming configurations leaves more area for heat loss from hot side and less area for heat transfer to the cold side resulting in smaller temperature gradient. The validity of semi-infinite solid assumption has been checked from the readings of thermocouple mounted near the non-contacting sides. Evidently, farthest nodes from the interface of configurations I and II, attain only 1 % of temperature change until 40 s. However this 1 % of temperature change is quite delayed for other four contact configurations (III-VI). The results from the non-conforming contact configurations (III-VI) illustrate that the temperature change of the farthest sensor becomes evident only after 70–80 s. The phenomenon of

different time span for 1 % of temperature change can be attributed to the beginning of surface heat transfer penetration to the interior locations much earlier in both the bodies of configurations I and II compared to other four configurations. These temperature curves substantiate the scope of the 1-D semi-infinite solid assumption for each configuration, and provide the allowable time duration which forms the basis of present analysis towards experimental estimation of $\dot{q}(t)$ using Eq. (3). To have a common perspective of analysis, all the subsequent results are shown only for a shorter durations (up to 40 s).

4.2. Transient interfacial heat flux

The stability of SEF algorithm depends on the uses of future time steps. However, the number of future time steps needs to be identified before estimating interfacial heat flux. Estimated heat flux along with the temperature drop variation has been presented to discuss the nature of interfacial heat transfer.

4.2.1. Effect of future time steps

The influence of future time steps (r) on the estimated heat flux is shown in Fig. 7. Typical curves of estimated heat flux for eight different values of r are shown for a single loading condition. Presented result clearly shows that uses of higher number of r smoothens and minimizes the scattering in estimated values of interfacial heat flux. Increasing r from 10 to 11 does not improves the result much; therefore 10 future time steps have been used in the present study for interfacial heat flux estimation.

4.2.2. Heat flux and temperature drop variations

The instantaneous heat flux variation with time has been estimated for all the six configurations under three axial loading conditions. Typical plots of transient interfacial heat flux along with the variation of interfacial temperature drop ($\Delta T(t)$) are depicted in Fig. 8 for all the six configurations under a common loading of 2000 psi. Here absolute value of heat flux estimation obtained from hot body (upper specimen), cold body (lower specimen), and the average of both have been presented together. In a way, the average of heat fluxes is generally regarded as the effective heat flux passing through the interface, henceforth only the average heat flux values, $\dot{q}(t)$ are used in the subsequent TCC analysis. The heat flux transient presented in Fig. 8 shows a clear peak for all the loading conditions representing a maximum value of heat fluxes termed as $\dot{q}_{max}$, which is attained shortly (within 4–6 s) after the contact of both the bodies. Most of the previous works related with the various manufacturing processes have showed the same trend [6–9], where sharp rise in the heat flux were linked with the high heat addition due to the good contact at the onset of various manufacturing processes.

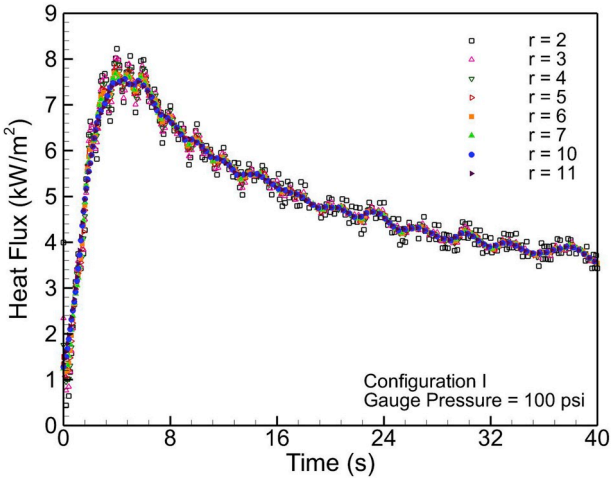

Fig. 7. Effect of future temperatures on heat flux estimation.

The increase till the peak in the heat flux curves is the zone where load is being applied to the contact. The increase in the axial load affects the deformation of the contact asperities causing growth in the real contact area. Once the applied load stabilizes and reaches the fixed value of gauge pressure, optimal contact is attained which results in maximum contact area at the interface. Therefore, the attainment of peak ($\dot{q}_{max}$) in the heat flux curve is also the indication of complete asperities deformation under the applied loading condition. This factor act favourably to accelerate the initial driving force and result in terms of sharp rise in heat flux up to the peak then a significant decrease in the driving force of heat transfer reflects consequential decay in the heat flux transient after the occurrence of peak. Interestingly once the heat flux attains the peak value, the gradient of the heat flux transient varies along with the interfacial temperature drop gradient, and afterward both the transient curve moves in tandem indicating a quasi-static equilibrium of heat flow. Furthermore, the time of occurrence of $\dot{q}_{max}$ is found to be of the same order (within 4 s) in all the six configurations.

A flat-flat contact represented by configuration I, exhibits conforming surface contact with interstitial substances, perfectly wetting all portions of the surfaces thus having maximum nominal area among all configurations. As inferred from Fig. 8, it is evident that in flat-flat contact, heat flux curves and its peak values for both of the hot and cold bodies superimposes with each other showing amount of heat loss from hot body is almost equal to the heat gain by cold body. Whereas, there exists a greater degree of mismatch in the heat flux curves and its peak values for both of the hot and cold bodies in configurations II-VI. Although configuration II also exhibits conforming surface contact but due to the curvilinear contacting surfaces the interstitial substance of the interface of upper body does not perfectly wet the contacting surface of the lower body, resulting in reduced contact area compared to flat-flat contact. Whereas other four contacts represented by configurations III-VI exhibiting line contacts in the decreasing order of contact width formed at their interfaces. Classical Hertz contact stress [34] explains that any typical line contact can be represented by a narrow rectangular strip, which exhibits the area contours around mating curvatures, whose size is directly influenced by the loading conditions, and the curvature of the mating surface as well. Therefore mismatch of heat fluxes in configurations III-VI can be explained on the basis of limited scope of heat flow to occur due to the narrowed contact area in line contacts. Henceforth, in addition to the micro surface constriction resistances, there exists an additional scope of macroscopic contact resistance due to these circumscribed area contours, resulting consequential increase in the overall contact resistance which restricts the heat flow at the interface. This explains well about the relatively lesser magnitude of overall heat flux magnitude and the significant heat loss from upper specimen to the lower specimen through these four non-conforming contacts.

4.3. Contact configurations and transient TCC

To study the effect of contact configurations on transient nature of TCC, results of transient TCC of all six configurations have been plotted together under each loading condition. Fig. 9 presents the nature of transient TCC for all six configurations under the loading of 100, 1000 and 2000 psi gauge pressure. All of the six curves show a rapid rise in $h(t)$ value immediately after the onset of contact, and thus follow similar trend till the attainment of peak as found in the heat flux transients curves (Fig. 8). This phenomenon can be attributed again to the enhanced capacity of heat transfer till the attainment of prescribed loading condition and to the rapid decrease in the interfacial temperature drops. In the configurations I and II, it can be observed that the estimated $h(t)$ increases rapidly and attains a stabilized value with very little variation shortly after the time of occurrence of $\dot{q}_{max}$. As discussed in the preceding section (section 4.2.2), once the interfacial load reaches the prescribed value, optimal contact takes place at the

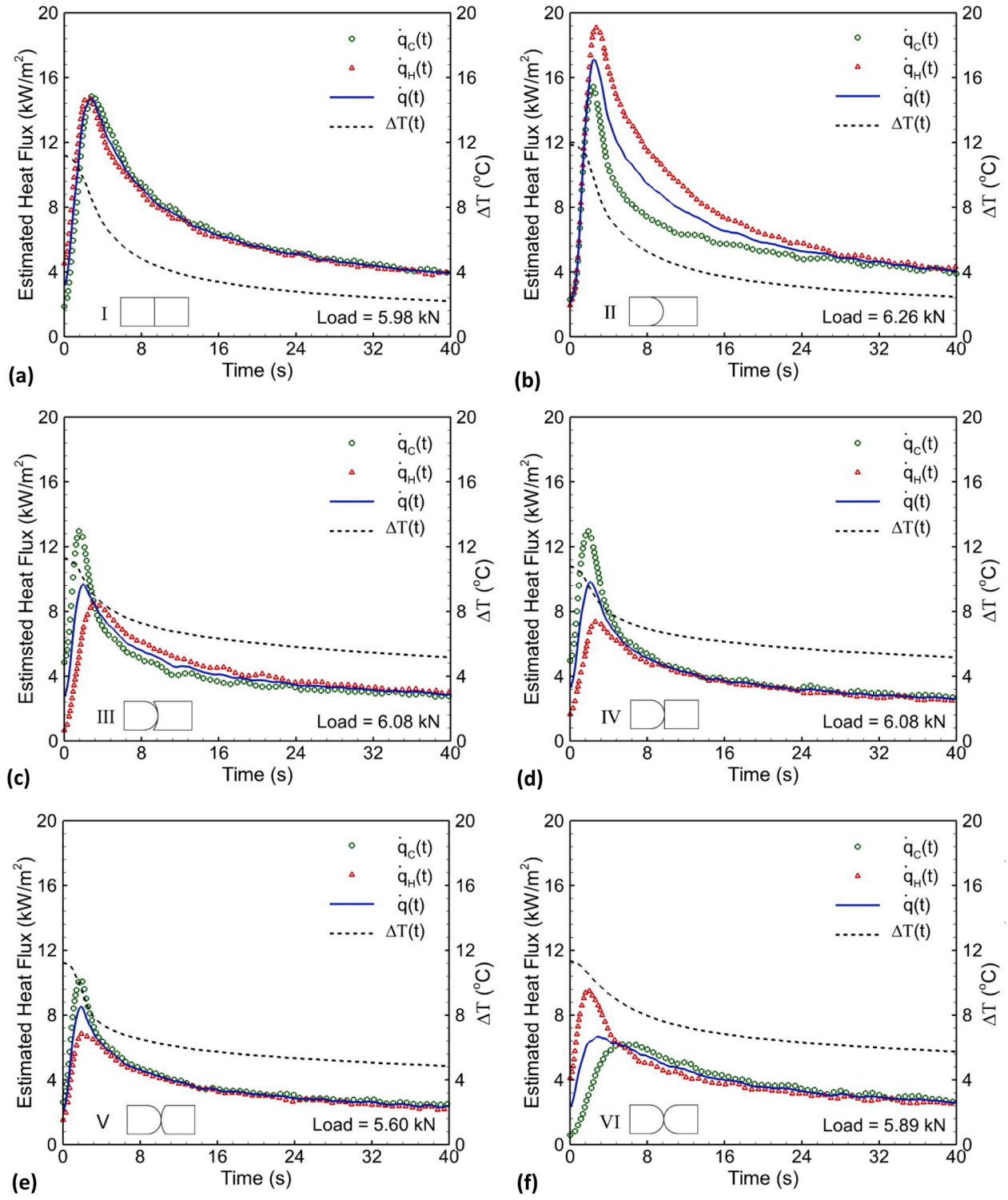

Fig. 8. A typical Transient heat flux and interfacial temperature drop variation in the contacting bodies of stainless steel of (a) configuration I, (b) configuration II, (c) configuration III, (d) configuration IV, (e) configuration V, and (f) configuration VI, under 2000 psi gauge pressure.

interface. It can also be seen in configurations I and II (Fig. 8) that the heat flux and interfacial temperature drop both decreases gradually, but interfacial temperature drop decreases at a much faster rate. Afterward both the curves attain a similar degree of gradient with time and moves in tandem with a fixed offset, and heat flow appears to be under quasi-static thermal equilibrium condition. Therefore, $h(t)$, which inherently represents the ratios of the heat flux transient and the interfacial temperature drop variation with time, becomes quite stable and attains a quasi-static state of thermal equilibrium in conforming configurations I and II. On the other hand curves of $h(t)$ exhibit completely different trend in other four non-conforming configurations (i.e., III-VI) representing line contacts. All four curves carry a clear dominant peak, which is attained shortly within half of the time span corresponding to the peak value of TCC obtained in configurations I and II. Once the peak in $h(t)$ has been attained for the non-conforming contacts, it decreases gradually and attains a steady and stable value during the period which

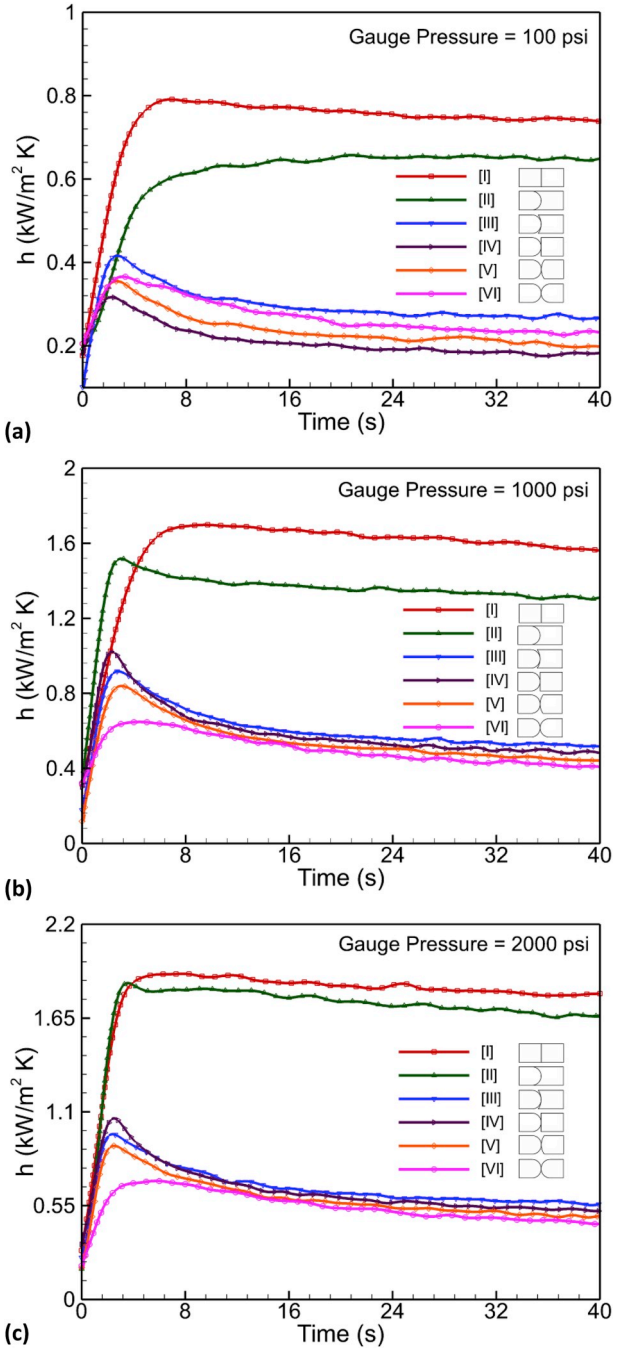

Fig. 9. Effect of contact configurations on transient TCC under three different axial loadings.

carries the quasi-static equilibrium of heat flow as seen earlier in Fig. 8.

Earlier analysis has already shown a different behaviour of heat flux transient against the interfacial temperature drop variation for non-conforming contacts (Fig. 8(c–f)). Where, contrary to the conforming contacts (Fig. 8(a and b)), interfacial temperature drop in non-conforming contacts (III-VI) decreases at much slower rate than the corresponding heat flux transient. Both of these curves moves in-tandem with fixed offset quite late (beyond two third of the total duration under representation (40 s), i.e. equivalent to ~27 s); only then it appears in a quasi-static equilibrium of heat flow condition during the remaining span of time (40 s), which is the permissible duration of span towards the viability of the present 1-D semi-infinite conduction solution. Henceforth a steady and stable value of $h(t)$ after the attainment of peaks is unlikely to appear in non-conforming contacts.

Similar to the earlier discussion on heat flux transients, the stabilized zone of $h(t)$ in configurations I and II is attained just after the peak due to the establishment of an optimal contact surface at the interface and a quicker balance between heat loss from upper and heat gain in lower body. Whereas the reason for the delayed attainment of quasi-static equilibrium in TCC for other four configurations (III-VI) can also be attributed toward the non-conforming nature of mating surfaces leading to circumscribed area contours in the form of typical line contacts, which act as the restricting passage for the heat lines during the initiations of the heat flow. Above study clearly states the impact of contact configurations in the nature of transient TCC. Thus conforming contacts show an early stabilization of transient TCC whereas non-conforming contacts initially present a clear peak and later a delayed stabilization of transient TCC. Now if the focus is laid on the stabilized zone of all the six configurations, it can be seen that except first three configurations (I-III), the magnitude of TCC for other three configurations (IV-VI) are not in order of their contact area at lower loading condition (i.e. 100 psi). The primary reason for this discrepancy is due to very low loading (100 psi ~0.17–0.32 kN) at interfaces of contact configurations. It has been a cumbersome task to apply a common low loading at all the interfaces of curvilinear contacts therefore even for small deviation in loadings can lead to a significant increase in contact area consequently leading to a deviation in TCC among different line contacts. The contact width calculated by using classical Hertz Contact Stress [34] and area formed by the rectangular strip for configurations III-VI has been presented in Table 2. It can be clearly inferred from the presented Table 2, as load increases from 100 to 1000 psi, apparent contact area increases significantly (upto 375%). At the same time increase of loading from 1000 to 2000 psi leads only a marginal increase in apparent contact area (upto 36%) in all four configurations.

Now to study the transient behaviour of $h(t)$ under higher loadings, same analysis has been performed again for all six configurations under 1000 and 2000 psi loadings and their results are shown in Fig. 9(b and c). Similar nature of $h(t)$ has been observed for conforming as well as non-conforming contacts. At higher loadings, not only the overall magnitude of $h(t)$ gets increased but any conflicts in stabilized value of TCC among line contacts exists at lower loading also get resolved. If stabilized zone from $h(t)$ curves can be considered as the representing TCC then transient TCC at 1000 psi loading shows that the magnitude of TCC are in increasing order according to the apparent contact area of configurations. Thus at similar loading conditions higher the apparent contact area higher the TCC. Enhanced loading (i.e. 2000 psi) at the interfaces reiterates the nature of transient TCC observed at lower loadings. Further, at higher loadings, there is minimal but distinct difference of stabilized TCC among all four line contacts (III-VI). The presented results clearly show a new insight in the understanding of the different nature of transient interfacial heat transfer occurs in different engineering application.

Table 2
Contact width and rectangular strip area for non-conforming contacts.

Configuration	Loading		Contact Width, μm	Specimen Thickness, mm	Rectangular Strip Area, mm^2
	psi	*kN*			
III	100	0.26	119.5	22.50	2.69
IV		0.18	63.6	22.50	1.43
V		0.29	65.4	22.50	1.47
VI		0.24	51.9	22.50	1.17
III	1000	3.83	454.0	22.50	10.22
IV		3.97	301.7	22.50	6.79
V		3.04	210.3	22.50	4.73
VI		3.81	208.8	22.50	4.70
III	2000	6.08	572.5	22.50	12.88
IV		6.08	373.2	22.50	8.40
V		5.60	285.1	22.50	6.42
VI		5.89	259.6	22.50	5.84

4.4. Transient versus steady state TCC

In this section, it would be interesting to highlight the concern raised earlier to get the steady state TCC from the transient TCC curve. In other words, predicting the steady state TCC estimate on the basis of transient temperature measurement. In this regard, it is necessary to compare the transient results with their corresponding steady state measurements. As discussed earlier present transient TCC estimate is based upon single thermocouple measurement which is mounted at 2 mm away from the interface, whereas steady state TCC has been estimated in two ways. One is the conventional way, where extrapolation of temperature profile is performed in order to obtain steady state at the interface, and the second is by calculating TCC on the basis of direct calculation of at 2 mm away from the interface (contacting side). As $h_{\Delta T\_\text{exptrp.}}$, considered the most reliable estimate of TCC, therefore its comparison with the transient TCC is obvious. Whereas, data taken for the calculation of , in the estimation of $h_{\Delta T\_\text{no exptrp.}}$ is from the same location where data for estimating of transient TCC has been taken (2 mm away from the contacting end), therefore both of these comparison also seems relevant under the given scenario. Variation of transient interfacial heat transfer coefficients for all six configurations with their respective $h_{\Delta T\_\text{no exptrp.}}$ as straight dotted line are shown together for comparison under three different loading conditions (i.e., 100, 100, and 2000 psi) in Fig. 10 and Fig. 11. The comparison of transient TCC with the conventional $h_{\Delta T\_\text{exptrp.}}$ and $h_{\Delta T\_\text{no exptrp.}}$ has been presented in Table 3. The discussion on the comparison between transient and steady state TCC has been first presented for conforming contacts and then for non-conforming contacts.

4.4.1. Conforming contacts

On the basis of graphical comparisons presented in Fig. 10 between transient TCC variation and $h_{\Delta T\_\text{no exptrp.}}$, it is reasonable to conclude that once the transient TCC value get stabilized in conforming contacts and attain quasi-static equilibrium state of heat flow, the flatter profile matches remarkably well with the $h_{\Delta T\_\text{no exptrp.}}$ (steady state TCC) values. Further, the effect of increase in axial load at the interface is observed in terms of the increase in the overall instantaneous TCC value due to the enhanced interfacial heat flux transient and sharp decay in instantaneous interfacial temperature drop. Similar phenomenon has been observed for all the three loading conditions.

A single value of TCC has been selected from the stabilized flatter profile of transient TCC curve. This stabilized value has been taken as a representative value of transient TCC and has been presented in the fourth coloumn of Table 3 for the two configurations (I and II). Maximum increase in TCC is observed when axial load increases from 100 to 1000 psi and afterward further increase in loading (i.e. 2000 psi) has smaller effect on TCC. Further based upon the comparison between stabilized values of $h(t)$ and $h_{\Delta T\_\text{no exptrp.}}$, it can be concluded that the quasi-steady state condition of the transient heat flow is successfully able to extract the steady-state TCC measurement. This can be treated as an important observation, and provides a plausible solution to predict the steady state TCC measurement on the basis of short duration based transient experiments. Contrary to the earlier experiments with flat-flat contact configurations [6,11,13,17] where tremendous ambiguity exists during the selection of representative value from the instantaneous TCC curve, present transient methodology provides a reliable outcome to correlate the transient TCC measurement with that of the steady state TCC value on the basis of simple 1-D solution of semi-infinite conduction problem.

4.4.2. Non-conforming contacts

The comparison between transient TCC variation and $h_{\Delta T\_\text{no exptrp.}}$ has been presented in Fig. 11 for four contact configurations. It can be inferred from the comparison that the peak value attained in the TCC curve which corresponds to the peak of heat flux transient i.e. $\dot{q}_{\max}$, cannot be taken as the representative value of TCC from the transient TCC curves. The match between the stabilized values of transient TCC with the steady state TCC, $h_{\Delta T\_\text{no exptrp.}}$ occurs quite late in the non-conforming contact configurations (III-VI) as against the conforming contacts (I-II). The stabilized value of transient TCC for four configurations has been presented in the fourth coloumn of Table 3. It can be observed that the value of transient TCC is remarkably low in non-conforming contacts than the conforming contacts.

Finally, comparison of stabilized value of $h(t)$ with the convention steady state TCC ($h_{\Delta T\_\text{extrp.}}$) has been made and results are shown in Table 3. It has been observed that the stabilized value of $h(t)$, which represents the quasi-steady state heat flow condition during transient run, does a not match well with $h_{\Delta T\_\text{extrp.}}$. It shows underpredictions of steady state TCC ($h_{\Delta T\_\text{extrp.}}$) in the range of 3.16–68.60% for different contact configurations The calculation of transient temperature gradient ($\Delta T(t)$), exactly at the interface, is physically impossible using intrusive measurement (thermocouples). Therefore underprediction of $h_{\Delta T\_\text{extrp.}}$, where is calculated exactly at the interface using extrapolation method, is obvious when it is compared with the stabilized value of $h(t)$.

In case of conforming contacts, considerable underprediction of $h_{\Delta T\_\text{extrp.}}$ by the stabilized value of $h(t)$ resulted as high as 68.60% whereas stabilized value of $h(t)$ matches will with $h_{\Delta T\_\text{no exptrp.}}$. This mismatch is mainly due to the significant difference between calculated steady state obtained by the extrapolation and obtained without extrapolation of the temperature profiles in the estimation of steady state $h_{\Delta T\_\text{extrp.}}$ and $h_{\Delta T_\text{no exptrp.}}$respectively. Whereas non-conforming contacts

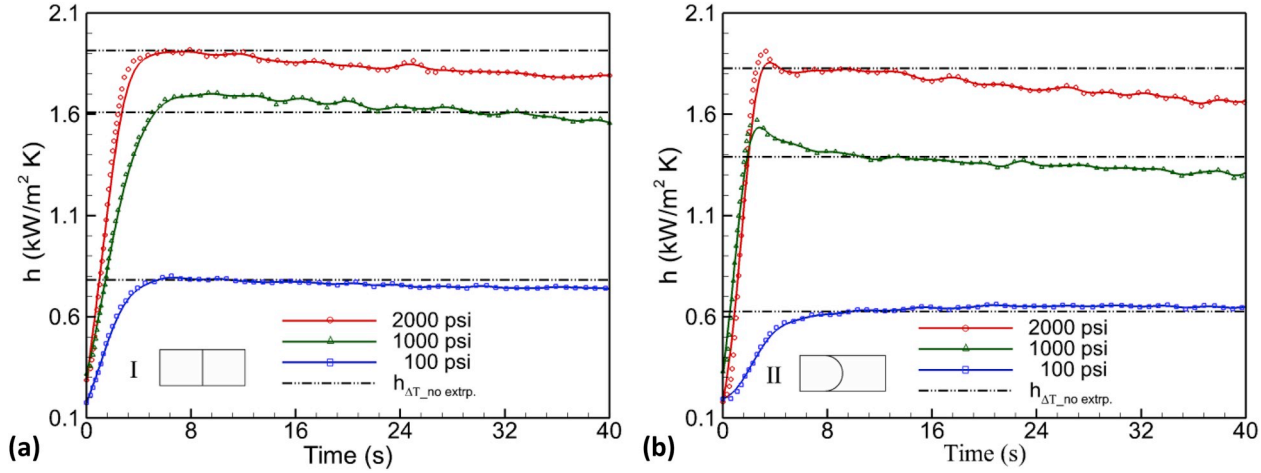

Fig. 10. Transient verses steady state TCC for two conforming contacts (a) configuration I, and (b) configuration II, placed under three axial loading conditions.

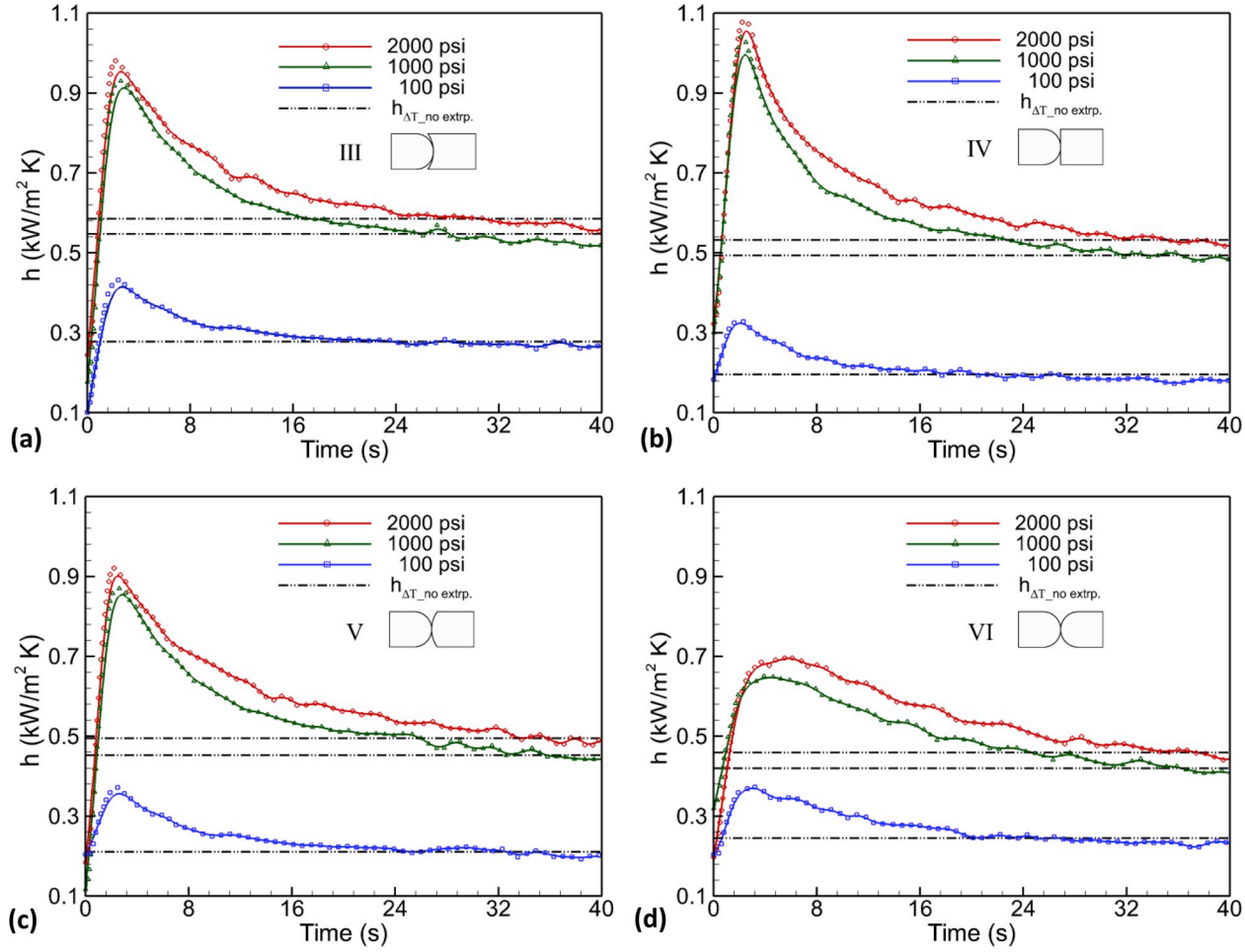

Fig. 11. Transient verses steady state TCC for four non-conforming contacts (a) configuration III, (b) configuration IV, (c) configuration V, and (d) configuration VI, placed under three axial loading conditions.

exhibit an interesting outcome of the comparison where underprediction of steady state TCC ($h_{\Delta T\_extrp.}$) get reduced drastically (maximum 6.85%). This finding is primarily due to the minimal difference between calculated steady state obtained by extrapolation and obtained without extrapolation of the temperature profiles in non-conforming contacts. However a larger underprediction in the results in all six configurations at higher loadings can also be attributed toward the increase in uncertainty of TCC estimate due to greater extrapolation errors for lower values of , and other associated factors at higher loadings [5].

Table 3
Comparison of estimated transient TCC with steady state TCC.

Configuration	Loading		Stabilized value of $h(t)$, kW/m^{2}K	$h_{\Delta T\_no\ exptrp.}$, kW/m^{2}K	$h_{\Delta T\_extrp}$, kW/m^{2}K	Underprediction of $h_{\Delta T\_extrp}$ by$h(t)$ (%)
	psi	*kN*				
I	100	0.17	0.782	0.782	1.072	27.05
II		0.32	0.625	0.618	0.739	15.43
III		0.26	0.278	0.278	0.297	6.40
IV		0.18	0.196	0.196	0.203	3.45
V		0.29	0.211	0.211	0.219	3.65l
VI		0.24	0.245	0.245	0.253	3.16
I	1000	3.34	1.610	1.610	3.205	49.77
II		3.92	1.389	1.419	2.435	42.96
III		3.83	0.547	0.547	0.586	6.66
IV		3.97	0.493	0.493	0.519	5.01
V		3.04	0.452	0.452	0.474	4.64
VI		3.81	0.420	0.420	0.439	4.33
I	2000	5.98	1.915	1.986	6.098	68.60
II		6.26	1.827	1.827	3.380	45.95
III		6.08	0.585	0.585	0.628	6.85
IV		6.08	0.532	0.532	0.564	5.67
V		5.60	0.495	0.495	0.522	5.26
VI		5.89	0.459	0.459	0.484	5.16

Conclusively, the above results prove the credibility of the present methodology to get the accurate estimation of steady state TCC with short duration transient experiments. It is also well understood that the under prediction of actual TCC is not due to the inability of the algorithm, rather due to the physical and practical limitation of sensors placement at the interface for the calculation of $\Delta T(t)$. Therefore, present methodology looks quite promising when used in conjunction with the modern high resolution optical based temperature mapping tools, which can correctly predict the temperature in the immediate vicinity of the interface, and therefore would be the scope of our upcoming research investigations.

5. Uncertainty analysis

The uncertainty of an entity depends on several independent variables. Error in thermocouples measurement would significantly impact the result. Therefore all thermocouples were in house calibrated with sophisticated calibrator before using them in the experimental facility. Error associated with thermocouples measurement has been corrected and nullified and has not been included in the error analysis. Uncertainty in estimating temperature drop for six configurations (i.e. I-VI) is ± 7.22, ±4.33, ±2.53, ±2.50, ±2.57, and ± 2.19 % respectively. Accuracy in the heat flux calculation from specimens depends on the thermal conductivity of specimens. Uncertainty in the measurement of thermal conductivity of specimens is ± 1.50 %. The heat loss from the specimen to the surroundings represents a major source of uncertainty in contact heat transfer experiments [35]. It has been observed that there is a dominance of lateral heat transfer over axial heat transfer in the line contacts (III-VI). This dominance is due to lesser nominal area of contact in line contacts compared to surface contacts. The limited nominal contact at the interface brings a favourable condition for the constricted axial heat flow and thus lead to increase in thermal loss to the environment. Inherently, this situation contributes for the greater temperature drop at the interface, and lead to rise in the heat loss to the surrounding. The maximum heat flux loss (% $\dot{q}_{\text{loss}}$) through upper test specimen for six contacts is ± 6.50,± 11.20, ±15.10, ±16.25, ±16.35, and ± 16.85 % respectively. Finally, based on the law of error propagation model by Holman [36], maximum overall uncertainty in steady state experimental TCC for six configurations (i.e. I-VI) have been estimated as ± 11.50, ±13.51, ±16.54, ±17.45, ±17.46 and ± 18.33 % respectively. It can be observed that, as the area of contact starts decreasing (surface to line) high level of uncertainty results in their TCC, due to a large magnitude of heat losses between the contacting bodies and ambient in the line contacts (III-VI) under similar loading conditions.

6. Conclusions

A new perspective on the nature of transient interfacial heat transfer occurring at the junction of metallic contacts has been presented by analysis the results obtained from transient and steady state experiments performed in a uniquely designed setup on six different geometric configurations. SFE algorithm based on single sensor measurements has been explored for the estimation of transient TCC between different contact configurations using 1-D semi-infinite conduction solution. Primary results of heat flux transient across six configurations present a clear peak, which has been attained shortly after the contact and also represent the maximum value of heat flux attained during the total duration of analysis. The attainment of peak is mainly due to the stabilization of loading condition leading to optimal contact at the interface. The transient heat flux presents a sharp decay after the peak, and the decrease in the instantaneous interfacial temperature drop value are concluded as the prime reason for this gradual decay. The gradient of the heat flux transient are found to vary along with the interfacial temperature drop gradient after suitable span of time, and afterward both the transient curve moves in tandem indicating a quasi-static equilibrium of heat flow. Conforming contacts attain the quasi-static equilibrium shortly after the occurrence of $\dot{q}_{\max}$, whereas it gets delayed for the nonconforming contacts. Results of TCC transient of different configurations show a definite effect of conforming and non-conforming contacts on the nature of transient TCC. Combined study of conforming and non-conforming contacts suitably explains why different engineering applications show different behaviour of transient TCC under similar thermophysical conditions. Conforming contacts exhibits a stabilized flatter profile of $h(t)$, whereas in non-conforming contacts a clear peak is evident and attainment of stabilized zone is quite delayed. Consequential curve of the transient TCC illustrates that the instantaneous TCC value get stabilized only during the typical quasi-static equilibrium state of heat flow, and this value of TCC matches remarkably well with the $h_{\Delta T\_\text{no exptrp.}}$ obtained on the basis of direct steady state interfacial temperature drop measurements. It has been inferred that the quasi-steady state condition of the transient heat flow is successful in evaluating the steady-state TCC measurement with greater reliability. This can be treated as an important observation, and provides a plausible solution to predict the steady state TCC measurement on the basis of short duration transient experiments. However, comparison between stabilized value of $h(t)$ and steady state TCC ($h_{\Delta T\_\text{extrp.}}$) calculated with extrapolation of temperatures exhibits underprediction as high as 69%. For sure, it advocates towards the implementation of the non-intrusive based optical techniques in order to obtain $\Delta T(t)$ exactly at the interface; however seeing the ease in implementation and associated cost of the experiment, present investigations with thermocouple can be regarded as the baseline experiment which provide valuable comparison between the transient and steady state results, and deals about the suitability of the present experimental methodology for the estimation of TCC between various contact configurations.

Acknowledgements

The authors gratefully acknowledge the financial support of the Bhabha Atomic Research Centre (BARC), India for initiating this research activity in Mechanical & Industrial Engineering Department (MIED) at Indian Institute of Technology (IIT) Roorkee, India.

Nomenclature

Fo	Fourier number
h	interfacial heat transfer co-efficient or TCCkW/m^{2}K
k	thermal conductivity, W/m K
L	length of a body, m
M	general time step index
$\dot{q}$	average interfacial heat flux, $\frac{\dot{q}_C + \dot{q}_H}{2}$, kW/m^2
$\dot{q}_{\text{C}}$	heat flux estimated from cold body, kW/m^2
$\dot{q}_{\text{H}}$	heat flux estimated from hot body, kW/m^2
% $\dot{q}_{\text{loss}}$	$\left(\frac{\dot{q}_{\text{H}}}{\dot{q}_{\text{H}} - \dot{q}_{\text{C}}}\right) \times 100$
R	radius, m
r	future time steps or number of future temperatures
t	time, s
T	temperature, °C
$\hat{T}$	calculated temperature, °C
x	spatial coordinate, m
Y	measured temperature, °C

Greek Symbols

	temperature drop at the interface, °C
α	thermal diffusivity, m^2/s
Φ	sensitivity coefficient, m^{2}K/W

Subscripts/Superscripts

extrp.	extrapolation, calculated exactly at the interface
no extrp.	no extrapolation, calculated at the nearest sensor from the

	interface
H	hot
C	cold
0	upper body in the configurations II to VI
2, 3, 4, 5, 6	lower body in the configuration II to VI respectively
i	initial
U, L	upper and lower body
max	maximum

References

[1] M.G. Cooper, B.B. Mikic, M.M. Yovanovich, Thermal contact conductance, Int J Heat Mass Tran. 12 (1969) 279–300.
[2] B.B. Mikic, Thermal contact conductance; theoretical considerations, Int J Heat Mass Tran. 17 (1974) 205–214.
[3] V.V. Rao, K. Bapurao, J. Nagaraju, M.V.K. Murthy, Instrumentation to measure thermal contact resistance, Meas Sci Technol. 15 (2004) 275–278.
[4] Y. Xiao, H. Sun, L. Xu, H. Feng, H. Zhu, Thermal contact conductance between solid interfaces under low temperature and vacuum, Rev Sci Instrum. 75 (2004) 3074–3076.
[5] A. Tariq, M. Asif, Experimental investigation of thermal contact conductance for nominally flat metallic contact, Heat Mass Tran. 52 (2016) 291–307.
[6] C. Fieberg, R. Kneer, Determination of thermal contact resistance from transient temperature measurements, Int J Heat Mass Tran. 51 (2008) 1017–1023.
[7] T.P.D. Rajan, K.N. Prabhu, R.M. Pillai, B.C. Pai, Solidification and casting/mould interfacial heat transfer characteristics of aluminum matrix composites, Compos Sci Technol. 67 (2007) 70–78.
[8] A. Plotkowski, M.J.M. Krane, The use of inverse heat conduction models for estimation of transient surface heat flux in electroslag remelting, J Heat Tran. 137 (2015).
[9] P. Fernandes, K.N. Prabhu, Comparative study of heat transfer and wetting behaviour of conventional and bioquenchants for industrial heat treatment, Int J Heat Mass Tran. 51 (2008) 526–538.
[10] B. Abdulhay, B. Bourouga, F. Alzetto, C. Challita, Development of an experimental procedure for thermal contact resistance estimation at the glass/metal contact interface, J Therm Sci Eng Appl. 6 (2014) 21006.
[11] Z. Zhu, L.W. Zhang, S.D. Gu, Experimental investigation of transient heat transfer between hastelloy C-276/narrow air gap/silicon steel, Exp Therm Fluid Sci. 45 (2013) 221–226.
[12] G. Ramesh, K.N. Prabhu, Heat transfer at the casting/chill interface during solidification of commercially pure Zn and Zn base alloy (ZA8), Int J Cast Met Res. 25 (2012) 160–164.
[13] Z. Malinowski, J. Lenard, M. Davies, A study of the heat-transfer coefficient as a function of temperature and pressure, J Mater Process Technol. 41 (1994) 125–142.
[14] B. Smith, T. Brunschwiler, B. Michel, Comparison of transient and static test methods for chip-to-sink thermal interface characterization, Microelectron J. 40 (2009) 1379–1386.
[15] B. Dongmei, H. Chen, T. Ye, Influences of temperature and contact pressure on thermal contact resistance at interfaces at cryogenic temperatures, Cryogenics 52 (2012) 403–409.
[16] B. Sponagle, D. Groulx, Measurement of thermal interface conductance at variable clamping pressures using a steady state method, Appl Therm Eng. 96 (2016) 671–681.
[17] Z. Zhu, L. Zhang, C. Zhang, R. Li, S. Gu, Experimental investigation of transient contact heat transfer between 300M and 5CrNiMo, Int J Heat Mass Tran. 96 (2016) 451–457.
[18] G.H. Ayers, Cylindrical Thermal Contact Conductance, M.S. Thesis Texas A&M University, Texas, 2003.
[19] S.S. Kumar, P.M. Abilash, K. Ramamurthi, Thermal contact conductance for cylindrical and spherical contacts, Heat Mass Tran. 40 (2004) 679–688.
[20] C.V. Madhusudana, Thermal conductance of cylindrical joints, Int J Heat Mass Tran. 42 (1999) 1273–1287.
[21] G.R. Mcgee, M.H. Schankula, M.M. Yovanovich, Thermal resistance of cylinder-flat contacts: theoretical analysis and experimental verification of a line-contact model, Nucl Eng Des. 86 (1985) 369–381.
[22] R. James, K. Rowe, D. Gary, J. Lock, M. Owen, Transient heat transfer measurements using thermochromic liquid crystal: lateral-conduction error, Int J Heat Fluid Flow 26 (2005) 256–263.
[23] M.N. Ozisik, H.R.B. Orlande, Inverse Heat Transfer: Fundamentals and Applications, Taylor and Francis, New York, 2000.
[24] K.A. Woodbury, S.K. Thakur, Redundant data and future times in the inverse heat conduction problem, Inverse Probl Eng. 2 (1996) 319–333.
[25] J. Beck, K. Woodbury, Inverse problems and parameter estimation: integration of measurements and analysis, Meas Sci Technol. 9 (1998) 839–847.
[26] J.V. Beck, B. Blackwell, C.R. St, Clair, Inverse Heat Conduction. Ill- Posed Problems, Wiley-Verlag, New York, 1985.
[27] V. Norouzifard, M. Hamedi, Experimental determination of the tool–chip thermal contact conductance in machining process, Int J Mach Tool Manufact. 84 (2014) 45–57.
[28] J.G. Stoltz, Numerical solution to an inverse problem of heat conduction for simple shapes, J Heat Tran. 82 (1960) 20–26.
[29] P.R.N. Childs, J.R. Greenwood, C.A. Long, Heat flux measuring techniques, Proc Inst Mech Eng. 213 (1999) 655–677.
[30] H.S. Carslaw, J.C. Jaeger, Conduction of Heat in Solids, Oxford University Press, Amen House, London, 1959.
[31] S. Kumar, A. Tariq, Determination of thermal contact conductance of flat and curvilinear contacts by transient approach, Exp Therm Fluid Sci. 88 (2017) 261–276.
[32] M. Asif, A. Tariq, Correlations of thermal contact conductance for nominally flat metallic contact in vacuum, Exp Heat Tran. 6152 (2016) 1–29.
[33] S. Kumar, A. Tariq, Steady state experimental investigation of thermal contact conductance between curvilinear contacts using liquid crystal thermography, Int J Therm Sci. 118 (2017) 53–68.
[34] J.E. Shigley, Mechanical Engineering Design, third ed., McGraw Hill, Inc., New York, 1977.
[35] C. V Madhusudana, Accuracy in thermal contact conductance experiments - the effect of heat losses to the surroundings, Int Commun Heat Mass Tran. 27 (2000) 877–891.
[36] J.P. Holman, Experimental Methods for Engineers, seventh ed., Tata McGraw Hill, New Delhi, 2001, pp. 51–60.